Synthesis, Solution Structure, and Biological Evaluation of Urokinase Type Plasminogen Activator (uPA)-Derived Receptor Binding Domain Mimetics

Niko Schmiedeberg,[†] Manfred Schmitt,[‡] Christian Rölz,[†] Vincent Truffault,[†] Martin Sukopp,[†] Markus Bürgle,[§] Olaf G. Wilhelm,[§] Wolfgang Schmalix,[§] Viktor Magdolen,[‡] and Horst Kessler*[,†]

Institut für Organische Chemie und Biochemie, Technische Universität München, Lichtenbergstrasse 4, D-85747 Garching, Germany, Frauenklinik der Technischen Universität München, Ismaninger Strasse 22, D-81675 München, Germany, and Wilex AG, Grillparzerstrasse 10B, D-81675 München, Germany

Received June 13, 2002

Tumor cell migration and metastasis in cancer are facilitated by interaction of the serine protease urokinase type plasminogen activator (uPA) with its receptor uPAR (CD 87). Overexpression of uPA and uPAR in cancer tissues is associated with a high incidence of disease recurrence and early death. In agreement with these findings, disruption of the protein−protein interaction between uPAR present on tumor cells and its ligand uPA evolved as an attractive intervention strategy to impair tumor growth and metastasis. For this, the uPAR antagonist *cyclo*[19,31][D-Cys^{19}]-uPA$_{19-31}$ was optimized to efficiently interrupt binding of uPA to cellular uPAR. First, the disulfide bridge of this lead compound was shifted and then the modified peptide was shortened from the amino and carboxy terminus to generate *cyclo*[21,29][Cys^{21,29}]-uPA$_{21-30}$. Next, *cyclo*[21,29][D-Cys^{21}Cys^{29}]-uPA$_{21-30}$ was yielded by changing the chirality of Cys^{21} to D-Cys^{21}. For analysis of uPAR binding activity, we employed competitive flow cytofluorometric receptor binding assays, using FITC-uPA as the ligand and U937 promyeloid leukemia cells as the cellular source of uPAR. As demonstrated for *cyclo*[21,29][D-Cys^{21}Cys^{29}]-uPA$_{21-30}$, the achieved peptide modifications maintained receptor binding activity ($IC_{50} = 0.04$ μM), which is close in order to that of the parent protein ligand, uPA ($IC_{50} = 0.01$ μM). A detailed NMR analysis with restrained and free molecular dynamics calculations in explicit H_2O exhibits a well-defined structure with characteristic features such as an ω-loop with two βI-turns about Lys^3, Tyr^4, Ser^6, and Asn^7. Hydrophobic clustering of the side chains of Tyr^4, Phe^5, Ile^8, and Trp^{10} is observed. Side chain mobility is analyzed with time-dependent distance restraints. The NMR structure of *cyclo*[21,29][D-Cys^{21}Cys^{29}]-uPA$_{21-30}$ is very similar to the previously reported structure of the amino terminal fragment of uPA. Systematic point mutations led to *cyclo*[21,29][D-Cys^{21}Nle^{23}Cys^{29}]-uPA$_{21-30}$, which still binds to uPAR but is resistant to proteolytic cleavage, e.g., by the tumor-associated serine proteases uPA and plasmin, and is stable in blood serum or plasma. In conclusion, small cyclic peptides were created, which mimic the structure and activity of the binding epitope of uPA to uPAR and which may serve as novel therapeutic agents in cancer metastasis.

Introduction

Metastasis of solid malignant tumors is initiated by detachment of tumor cells from the primary tumor, invasion of tumor cells into the surrounding extracellular matrix and into blood/lymphatic vessels, followed by extravasation from the vessels and reimplantation at distant loci. Tumor cell migration and invasion into the surrounding extracellular matrix is facilitated by a variety of proteolytic enzymes:[1−3] matrix metalloproteinases (MMPs), including collagenases, gelatinases, and stromelysins; cysteine proteases including cathepsins B and L; and serine proteases such as plasmin and the urokinase type plasminogen activator (uPA).

In cancer, plasmin, its activator uPA, the cell surface-associated receptor for uPA (uPAR, CD 87), and the two uPA inhibitors PAI-1 and PAI-2 are focused to the tumor cell surface inducing cell proliferation, chemotaxis, cell motility, and migration.[4] Clinical studies have clearly demonstrated that overexpression of uPA, PAI-1, or uPAR is associated with a high incidence of disease recurrence and early death.[5] In agreement with these findings, disruption of the protein−protein interaction between uPA and its receptor evolved as an attractive strategy to inhibit or diminish tumor growth and metastasis.[6−8]

The receptor binding region of uPA is located between amino acids 12 and 32 within the so-called growth factor domain (GFD) of uPA.[9,10] Synthetic linear and cyclic peptides of this sequence compete with naturally occurring uPA for binding to cellular uPAR.[9−12] Recently, we designed the cyclic uPA-derived peptide *cyclo*[19,31]-[D-Cys^{19}]-uPA$_{19-31}$, which sustains a high uPAR binding activity in the nanomolar range despite its "illegitimate" disulfide bond Cys^{19}−Cys^{31}.[11,12] Starting from this lead compound, we generated smaller cyclic high-affinity uPAR binding peptidomimetics with binding activities comparable to that of full-length uPA, with the potential to serve as novel therapeutics for the treatment of uPAR-positive cancer patients.

* To whom correspondence should be addressed. Tel: +49-89-289 13300. Fax: +49-89-289 13210. E-mail: Kessler@ch.tum.de.
[†] Technische Universität München.
[‡] Frauenklinik der Technischen Universität München.
[§] Wilex AG.

10.1021/jm020254q CCC: $22.00
Published on Web 10/08/2002

In cases where only small parts of the protein are responsible for biological activity, such as for the uPA/uPAR interaction, it is self-evident that peptide fragments mimicking its biologically active region represent an attractive therapeutic agent. To date, the number of peptide mimetics used in cancer therapy is rather low, although these compounds may represent the starting point for further reduction in size and, by stabilizing their bioactive conformation, increased biological activity, thereby leading to drugs suitable for clinical use.

Results and Discussion

Shortened uPA Peptides, Modifications, and Biological Activities. The minimum biologically active fragment of a receptor-directed peptide ligand, chosen by systematic deletions starting from the C and/or N terminus of the parent binding protein, often possesses only a fraction of the binding potency of the intact protein. One of the main reasons for that is the high flexibility of linear peptides, which are less rigidified as if they were part of a protein secondary structure. The introduction of constraints that limit the conformational freedom of the peptide may then help to regain biological activity or even may surplus the activity of the parent protein ligand if the biologically active conformation (matched case) is tethered.[13] Peptide analogues, containing a structural constraint that restricts the conformational space available for a certain residue or a group of residues by backbone to/or side chain cyclization, represent powerful molecules in search for the biologically active conformation.[11] Furthermore, in the case of side chain to side chain cyclization, side chain positions in the peptide have to be identified that are not mandatory for receptor binding activity and thus can be replaced by a functional group capable of a ring-closing reaction.

According to the structure of the human aminoterminal fragment of uPA (ATF, receptor binding domain, uPA_{1-136}) solved by Hansen et al.[14] by NMR, the region between Thr^{18} and Asn^{32} consists of a flexible, seven residue ω-loop (Asn^{22} to Ile^{28}) connected to a double-stranded, antiparallel β-sheet (between Thr^{18}–Ser^{21} and His^{29}–Asn^{32}). The C^{α}-atoms of Cys^{19} and Cys^{31} are in close proximity (average distance 6.1 Å) but form disulfide bonds with different cysteines (Cys^{11}–Cys^{19} and Cys^{13}–Cys^{31}) (Figure 1).

To determine the minimal uPAR binding region of uPA, a series of cyclic peptides were synthesized by shifting the disulfide bridge and successively shortening the lead compounds *cyclo*[19,31]-uPA_{19-31} **1**[11] and *cyclo*[19,31][D-Cys^{19}]-uPA_{19-31} **2**[12] from the amino and carboxy terminus. This strategy lead to peptide *cyclo*-[21,29][$Cys^{21,29}$]-uPA_{21-30} **3** as the new lead compound for further optimization regarding its uPA receptor binding activity. With the same approach as for peptide **1**, the systematic substitution of each amino acid residue in peptide **3** by alanine indicated that side chains of Cys^{21} and Cys^{29} (also leads to linear peptides), Tyr^{24}, Phe^{25}, Ile^{28}, and Trp^{30} are essential for its receptor binding activity, whereas other positions such as Asn^{22} and Asn^{27} apparently do tolerate substitutions by alanine without major loss of activity (Figure 1). However, some of the multiple alanine replacements resulted in a nearly complete loss of receptor binding activity. By

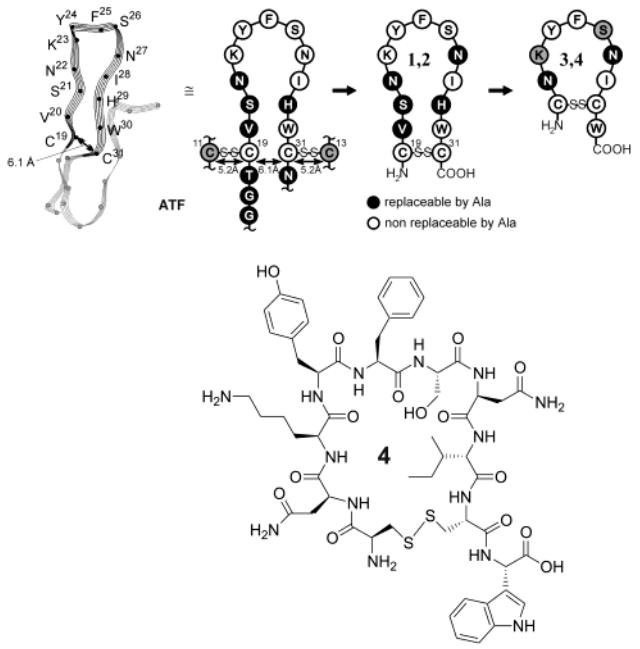

Figure 1. Design of synthetic cyclic peptides based on the receptor binding sequence of uPA. Cyclization of the receptor binding sequence of uPA (region encompassing amino acids 19−31 of ATF) or a variant thereof and substitution of L-Cys by D-Cys at position 19 (peptide **2**) or 21 (peptide **4**) generates lead structures *cyclo*[19,31]-uPA_{19-31} **1**, *cyclo*[19,31][D-Cys^{19}]-uPA_{19-31} **2**, *cyclo*[21,29][$Cys^{21}Cys^{29}$] uPA_{21-30} **3**, and *cyclo*[21,29]-[D-$Cys^{21}Cys^{29}$]-uPA_{21-30} **4**. Relative binding activities toward the cell surface receptor uPAR (CD87) based on alanine scan peptides are depicted as black (highly active), gray (moderate activity), or white (inactive) circles.

subsequent systematic substitution of each amino acid in peptide **3** by the corresponding D-amino acid, we made an effort to improve the rigidity of the peptide by introduction of structural elements such as β-turn motifs and analyzed the impact of the modified stereochemical orientation of the amino acid side chain on receptor binding activity.

Toward this end, inverted stereochemical orientation of the amino acid side chains at positions Asn^{22}, Tyr^{24}, Phe^{25}, and Ile^{28} lead to inactive peptides with the exception of the C-terminal Trp^{30}, which could be replaced by its D-isomer (Figure 2). In this D-Trp^{30} peptide, the receptor binding activity is about three times weaker than that of peptide **3** with L-Trp^{30} in the C-terminal position. This observation can be explained by the rotational freedom of the exocyclic amino acid enabling the aromatic side chain to adopt nearly every conformation required for receptor−ligand interaction (see also the section on Solution Structure and Dynamics) of *cyclo*[21,29][D-$Cys^{21}Cys^{29}$]-uPA_{21-30} **4**. Substitution of L-amino acids in peptide **3** by D-amino acids at positions Asn^{22}, Lys^{23}, Ser^{26}, and Asn^{27} yielded peptides with strongly reduced receptor binding affinity (IC_{50} > 30 μM) indicating a perturbation of the bioactive conformation of the cyclic peptide. Thus, stereochemical inversion of side chain residues in peptide **3** reduces receptor binding affinity, regardless of whether the corresponding amino acid side chains are required for receptor binding or not.

In contrast, stereochemical modification at the bridging Cys^{21}–Cys^{29} generated some highly biologically active cyclic peptides with *cyclo*[21,29][D-$Cys^{21}Cys^{29}$]-

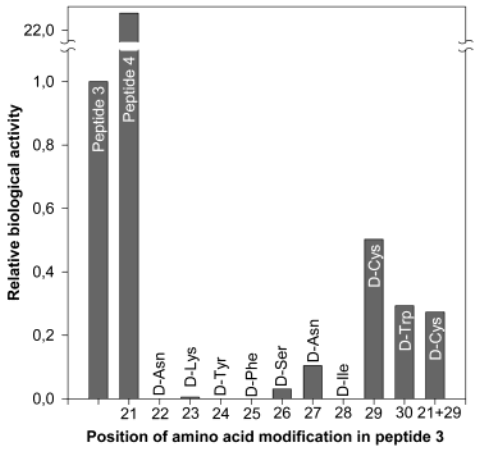

Figure 2. D-Amino acid substitution in *cyclo*[21,29][Cys^{21}-Cys^{29}]-uPA$_{21-30}$. Influence of D-amino acid substitution in *cyclo*[21,29][Cys^{21}Cys^{29}]-uPA$_{21-30}$ **3** on the capacity to inhibit binding of FITC-uPA to uPAR on U937 cells as assessed by FACS and related toward peptide *cyclo*[21,29][Cys^{21}Cys^{29}]-uPA$_{21-30}$ **3**.

uPA$_{21-30}$ **4** displaying a relatively high uPAR binding activity with an IC$_{50}$ of 0.04 μM as compared to 0.9 μM for the L-isomer **3**. This finding is in agreement with that for peptide **1** in which the introduction of D-Cys at position 19 of the 13-mer *cyclo*[19,31]-uPA$_{19-31}$ **1** (IC$_{50}$ = 0.7 μM) resulted in the much more active peptide *cyclo*[19,31][D-Cys^{19}]-uPA$_{19-31}$ **2** (IC$_{50}$ = 0.2 μM).[12] Although not predictable, the increased activity in the D-Cys^{19} analogue (peptide **2**) may be due to relocation of the disulfide bridge from Cys^{11}−Cys^{19} and Cys^{13}−Cys^{31} to Cys^{19}−Cys^{31}, which strongly influences the stereochemical orientation of the corresponding N terminus, which obviously can be brought back into the correct binding position by the Cys^{19}−D-Cys^{19} mutation. The same principle is valid for the smaller 10-mer cyclic peptides **3** and **4** and is consistent with the biological significance of the amino terminus (see N-terminal modifications below). In contrast, the inversion of the stereocenter at Cys^{29} in peptide **3** (and also Cys^{31} in peptide **1**) resulted in decreased receptor binding activity and can be explained by the fact that the exocyclic indole ring of Trp^{30} no longer is able to adopt the optimal position for receptor binding since the C-terminal carboxylate group is not important for biological activity (see C-terminal modifications below). The inversion of the stereochemical orientation of Cys^{21} in the small cyclic peptide **3** yielding peptide **4** lead to a more pronounced difference regarding the biological activities of peptides **3** and **4** when compared with peptides **1** and **2**. The resulting high-affinity uPA mimic peptide **4** displays a binding reactivity with cellular uPAR (IC$_{50}$ = 0.04 μM) that is only about four times weaker than that of the natural ligand, uPA (IC$_{50}$ = 0.01 μM), and thus is one of the most active synthetic uPAR antagonists known to date.[15−18]

Introduction of all possible double and triple D-amino acid substitutions into peptide **4** at all of the D-isomer-tolerating positions resulted in peptides with strongly decreased receptor binding properties as compared to lead peptide **4** (data not shown). In another cycle of optimization, we tried to increase the conformational rigidity of cyclic peptides **3** and **4** and thereby to stabilize the biologically active conformation by synthesis of peptides bearing all possible combinations of D- or L-Cys- and D- or L-Pen residues in the bridging positions 21 and 29. However, none of these modifications resulted in a peptide with an improved receptor binding activity as compared to *cyclo*[21,29][D-Cys^{21}Cys^{29}]-uPA$_{21-30}$ **4**. Introduction of Pen residues into the molecule either destabilized the most active conformation or stabilized a mismatched inactive conformation. Compounds presenting with similar biological activity are those bearing at least an amino acid with a D-configuration in position 21 and an L-amino acid in position 29.

Furthermore, chemical modifications were performed involving the N and C terminus of peptide **4** to evaluate the significance of the amino and carboxylate group for receptor binding. This is of importance, as these positions are target sites for chemical modifications, e.g., attachment of tags for the spectroscopic or immunologic visualization of uPAR ligands in biological systems or for the oligomerization via linkers or dendrimers for clustering studies. Because these modifications can be introduced in certain positions during solid phase peptide synthesis without employing a further orthogonal protecting strategy, this approach would represent an easy access to establish such a group of compounds.

Deletion of the C-terminal carboxylic group in *cyclo*-[21,29][D-Cys^{21}Cys^{29}]-uPA$_{21-30}$ **4** as well as conversion of peptide **4** to a primary and secondary (amino hexanoic acid) C-terminal peptide amide entirely retained receptor binding activity (data not shown). Thus, the C terminus seems to be well-suited for further modifications such as tagging with marker molecules or linkers. In contrast, the N-terminal residue in peptide **4** is much more sensitive to modification, including acetate capping or deletion of the N-terminal amino group (substitution of Cys^{21} by 2-mercaptoacetic-, 3-mercaptopropionic, and *rac*-2-mercaptopropionic acid). Such peptides display a complete loss of receptor binding activity. Although there is no immediate rational explanation for this finding, ongoing studies indicate that a positive charge is required, at least in the region of the N terminus, since elongation of peptide **4** by Val^{20}, thereby yielding peptide *cyclo*[21,29][D-Cys^{21}Cys^{29}]-uPA$_{20-30}$, retains receptor binding activity. Acetylation at the N terminus of this peptide results in strongly decreased receptor binding activity, and in the case of the highly active parent peptide *cyclo*[19,31]-uPA$_{19-31}$ **1**, the positive charge of the amino group is even shifted by two more residues. Salt bridge formation between the C and the N terminus, stabilizing the bridging region in peptide **4**, can be ruled out since C-terminal modification did not influence the receptor binding activity at all (see above) and such a motif is not seen by NMR in peptide **4** in water.

Structural Characterization of *cyclo*[21,29][D-Cys^{21}Cys^{29}]-uPA$_{21-30}$ by NMR and Molecular Dynamics (MD). The three-dimensional (3D) structure of peptide **4** with its high activity and relatively small ring size was of special interest to explore. Whereas in linear peptides and large cyclic peptides considerable mobility can be expected, the sensitivity for stereochemical inversion of certain amino acid side chains (as found in the D-scan of peptides **3** and **4**) already pointed to some rigidity of this cyclic peptide. Hence, it was our goal to correlate its conformation with the corresponding recep-

Table 1. ^{1}H Chemical Shifts (ppm) of *cyclo*[21,29][D-Cys^{21}Cys^{29}]-uPA$_{21-30}$ **4** in Water at 280 K

residue	H^N	H^α	H^β	H^γ	H^δ	H^ϵ	miscellaneous
D-Cys^1		3.81	2.62/3.26				
Asn^2	8.57	4.51	2.62/2.79		6.99/7.38		
Lys^3	8.74	3.73	1.33/1.45	0.54/0.79	1.24	2.57	7.32 (HN^ϵ)
Tyr^4	8.03	4.16	2.52/2.62				6.86 ($H^{2,6}$)
							6.57 ($H^{3,5}$)
Phe^{5,a}	7.59	4.61	2.46/3.12				6.99 ($H^{2,6}$)
							7.06 ($H^{3,5}$)
Ser^6	8.40	3.91	3.70/3.79				
Asn^7	8.00	3.97	2.34/2.86		6.79/7.48		
Ile^8	7.42	3.76	1.56	0.91/1.16 (CH_2)	0.48		
				0.42 (CH_3)			
Cys^9	8.31	4.58	2.74/3.01				
Trp^{10}	7.97	4.47	2.98/3.08				9.76 (H^1)
							6.91 (H^2)
							7.27 (H^4)
							6.77 (H^5)
							6.77 (H^6)
							7.05 (H^7)

[a] Chemical shifts of aromatic protons were assigned using the NOESY spectrum. δ(Phe^{5}H^4) could not be assigned unambiguously due to signal overlap.

tor binding loop in naturally occurring uPA to get insights for further peptidomimetic design. The solution structure of the most active uPAR antagonist **4** was determined by NMR solution spectroscopy in water. For the sake of clarity, the following residues of *cyclo*[21,29]-[D-Cys^{21}Cys^{29}]uPA$_{21-30}$ **4** are numbered from 1 (N terminus) to 10 (C terminus), while for the corresponding amino acid residues of ATF the original numbering is retained.

NMR Assignments. The ^{1}H chemical shifts of peptide **4** (Table 1) were assigned from analysis of the correlation spectroscopy (COSY) and nuclear Overhauser enhancement spectroscopy (NOESY) spectra. At first, frequencies of nonaromatic protons of each of the amino acid spin systems were determined using the COSY spectrum. Next, frequencies of aromatic protons were obtained from the NOESY spectrum. To this end, the chain of strong nuclear Overhauer effects (NOEs) between adjacent protons in each aromatic amino acid side chain was traced, starting from the H^β protons. Finally, the sequential order of the amino acid spin systems was determined using characteristic H^α_i—H^N_{i+1} NOEs as well as interresidue side chain NOEs. A comparison of the obtained ^{1}H chemical shifts with the corresponding random coil values[19,20] revealed a considerable upfield shift for Lys^3 (random coil chemical shifts are given in parentheses; H^β: 1.33, 1.45 (1.76, 1.85); H^γ: 0.54, 0.79 (1.45); H^δ: 1.24 (1.70)) and Ile^8 (γCH_3: 0.42 (0.95), δCH_3: 0.48 (0.89)) side chain protons, which is due to aromatic ring systems adjacent in space (see the Structure section).

NMR-Derived Structure Parameters. A total of 110 unambiguous NOE-derived distance restraints was obtained from analysis of the NOESY spectrum, including 30 nontrivial intraresidue, 40 sequential, 25 short-range ($|i - j| < 5$, where i and j are residue numbers), and 15 long-range ($|i - j| \geq 5$) NOEs. Because of signal overlap in the two-dimensional (2D) NOESY spectrum, some structural information is lost (see similarity of chemical shift values given in Table 1). A histogram of the NOE restraints for each residue is shown in Figure 3. Aside from NOE-derived distances, nine $^3J(H^NH^\alpha)$ (Table 2) and an almost complete set of $^3J(H^\alpha H^\beta)$ (Table 3) coupling constants were obtained from analysis of the COSY and ECOSY spectra. NOESY signal overlap and/

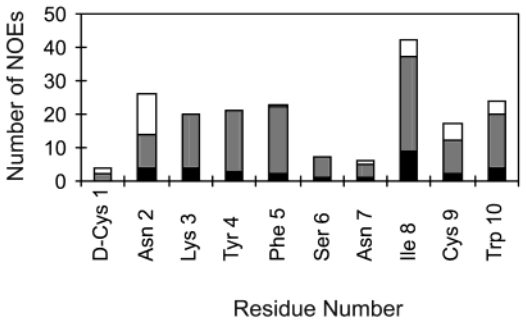

Figure 3. Histogram of NOE-derived distance restraints per residue. Intraresidue (black), short-range (gray; $1 \leq |i - j| < 5$, where i and j are residue numbers of participating residues), and long-range (white; $|i - j| \geq 5$) NOEs are given.

Table 2. $^3J(H^NH^\alpha)$ (Hz) of *cyclo*[21,29][D-Cys^{21}Cys^{29}]-uPA$_{21-30}$ **4** in Water at 280 K[a]

residue	$^3J(H^NH^\alpha)_{exp}$	$^3J(H^NH^\alpha)_{calcd}$
Asn^2	9.1	7.1 ± 2.3
Lys^3	7.1	5.3 ± 2.0
Tyr^4	11.3	8.0 ± 1.9
Phe^5	11.9	9.7 ± 1.3
Ser^6	8.7	3.9 ± 3.2[b]
Asn^7	9.1	6.5 ± 2.5
Ile^8	8.6	5.6 ± 2.4
Cys^9	8.7	9.6 ± 1.1
Trp^{10}	9.4	8.8 ± 1.7

[a] NMR-derived values and the corresponding values calculated from the rMD trajectory are given. Note that $^3J(H^NH^\alpha)$ was not employed as a restraint during the rMD simulations. [b] Small value with large standard deviation due to smeared distribution between $\phi = -60°$ and $\phi = 60°$.

or averaged $^3J(H^\alpha H^\beta)$ coupling constants due to side chain rotation (Table 3) did not allow for diastereotopic assignment of H^β. In addition to NOE distances and vicinal coupling constants, temperature dependencies of the chemical shifts from six out of a total of nine backbone amide protons were obtained from the temperature series of one-dimensional (1D) spectra.

Conformational Space Sampling. Only one family of backbone conformations was observed during conformational space sampling in vacuo using X-Plor (average backbone RMSD 0.6 Å from the family representative for residues 2—8). The considerable amount of signal overlap in the 2D NOESY spectrum overlap gives rise

Table 3. $^3J(H^\alpha H^\beta)$ (Hz) of *cyclo*[21,29][D-Cys^{21}Cys^{29}]-uPA$_{21-30}$ **4** in Water at 280 K[a]

residue	$^3J(H^\alpha H^\beta)_{exp}$	$^3J(H^\alpha H^\beta)_{calcd}$
D-Cys^1	4.5, 10.2	9.2 ± 4.3 (proS)
		4.6 ± 1.7 (proR)
Asn^2	4.6, 9.2	12.1 ± 1.6 (proS)
		3.1 ± 0.9 (proR)
Lys^3	6.3, 6.4	7.8 ± 5.0 (proS)
		4.6 ± 2.4 (proR)
Tyr^4	6.0, 10.3	3.8 ± 1.2 (proS)
		3.5 ± 1.2 (proR)
Phe^5	6.4, 9.0	3.1 ± 1.7 (proS)
		11.8 ± 2.5 (proR)
Ser^6	both ca. 7.0 (overlapped)	2.6 ± 0.7 (proS)
		5.1 ± 1.3 (proR)
Asn^7	7.4, 7.8	12.0 ± 1.1 (proS)
		2.4 ± 0.7 (proR)
Ile^8	6.8	6.9 ± 4.5
Cys^9	5.3, 9.5	8.8 ± 4.2 (proS)
		5.1 ± 4.6 (proR)
Trp^{10}	6.5, 7.5	3.0 ± 1.0 (proS)
		6.0 ± 3.5 (proR)

[a] NMR-derived values and the corresponding values calculated from the rMD trajectory are given. Because of NOESY signal overlap, no diastereotopic assignment could be made. Note that $^3J(H^\alpha H^\beta)$ was not employed as a restraint during the rMD simulation.

to ambiguous distance restraints. However, ambiguous distance restraints cannot be treated in the current version of the DISCOVER program, which is used for subsequent refinement. To probe whether the set of ambiguous distance restraints influences the convergence of the X-Plor runs, 3D structures were generated, with and without incorporation of ambiguous distance restraints. The results are virtually identical (backbone RMSD between structural representatives of 0.5 Å for residues 2−8). Thus, the set of unambiguous distance restraints already contained the principal structural information. Therefore, only unambiguous distance restraints were employed in the refinement stage.

Structural Refinement. The single structural representative obtained during conformational space sampling was refined in the course of 200 ps restrained MD (rMD) simulations in a cubic cell of 35 Å filled with explicit water molecules (see Experimental Section). To obtain average properties, two simulations were performed, starting from the same system configuration but for different initial velocities (Figure 4). Both rMD simulations lead to similar results (backbone RMSD between energy-minimized average structures 0.3 Å for residues 2−8). To probe the stability of the rMD structure, one simulation was resumed in absence of restraints for another 200 ps in the water cell (free MD, fMD). Inspection of the Ramachandran plots of the fMD trajectory (not shown) reveals that the rMD conformation is retained, a finding that is illustrated by the backbone RMSD between the energy-minimized average structures of both simulations (0.9 Å for residues 2−8).

According to analysis of the joint rMD trajectories (in the following denoted as rMD trajectory), the average violation of NOE-derived distance restraints is 0.1 Å, with no single distance restraint violated by more than 0.5 Å. Although coupling constants were not employed as restraints in the refinement stage, $^3J(H^N H^\alpha)$ calculated from the rMD trajectory are close to their experimental values (Table 2). Deviations by more than 2 Hz are interpreted in terms of the steep gradient of the

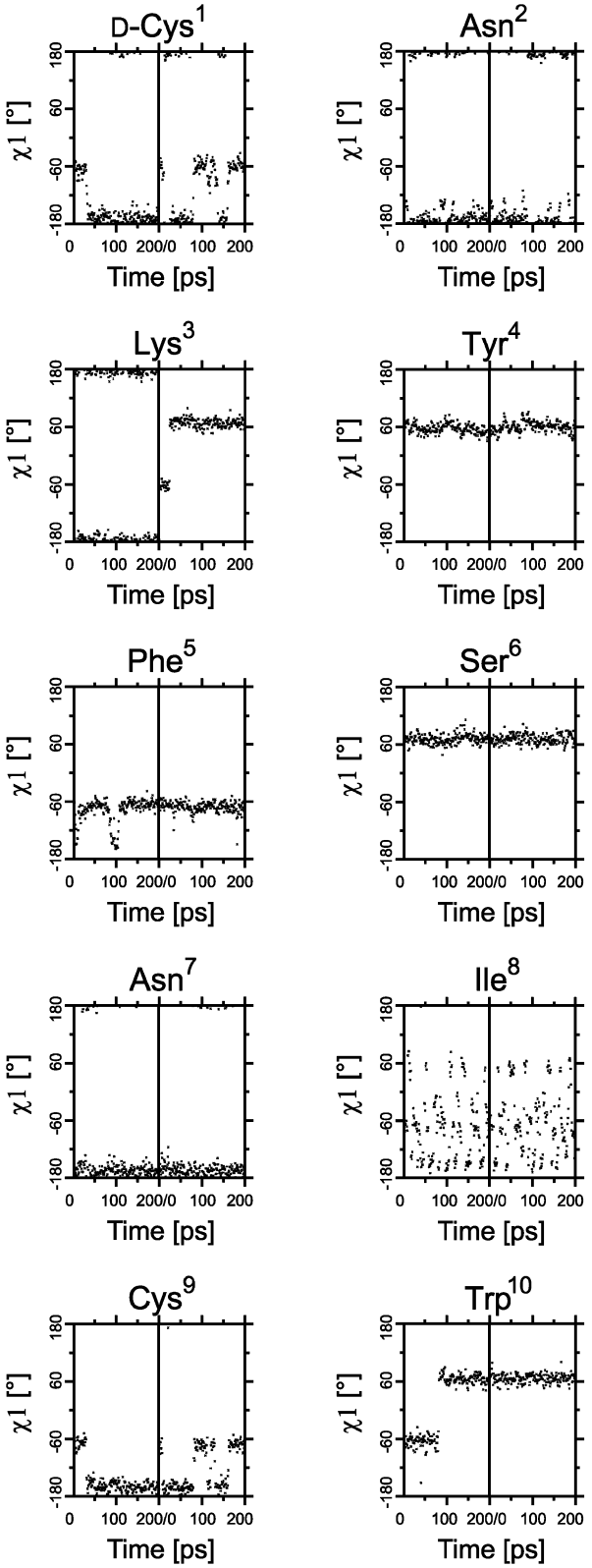

Figure 4. MD simulation. χ^1 angles in the course of the two 200 ps rMD simulations starting from different initial velocities. Each plot is split by a vertical line, displaying the data of simulations 1 and 2 on the left-hand and the right-hand side, respectively.

corresponding Karplus curve at $\phi = -80 \pm 30°$ (curve not shown). Similar considerations apply to $^3J(H^\alpha H^\beta)$. Despite the fact that no diastereotopic assignment of H^β was possible, a comparison of calculated vs experi-

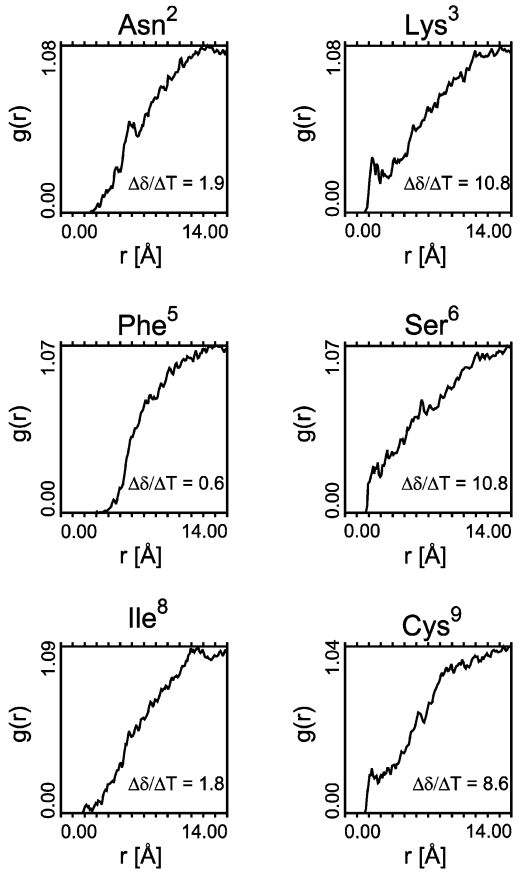

Figure 5. Radial distribution functions $g(r)$ of water oxygens around backbone amide protons. A steep rise of $g(r)$ at $r = 2.0$ Å, as observed for Lys[3], Ser[6], and Cys[9], indicates solvent exposure of these amide protons. The gradual rise of $g(r)$ seen in the plots for Asn[2], Phe[5], and Ile[8] results from shielding of these amide protons from solvent, accomplished by intramolecular hydrogen bonds or vicinity of side chains. Experimentally determined temperature dependencies of the amide proton chemical shifts ($\Delta\delta/\Delta T$ [-ppb/K], see plots) correlate well with the calculated radial distribution functions.

mental values of $^3J(H^\alpha H^\beta)$ yielded similar pairings (Table 3), suggesting that the side chain rotamer distribution is correctly reproduced by the rMD trajectory. Deviations occur for Tyr[4], Ser[6], Asn[7], and Trp[10]. In the case of Ser[6], no NOE-derived distance restraints were available due to signal overlap. Therefore, the calculated rotamer distribution merely reflects the force field preferences.

This is also true for Asn[7], where NOEs to the H^β are present but because of the fact that the DISCOVER program cannot handle pseudo atoms under periodic boundary conditions, act on the C^β atom, thereby eliminating their influence on the χ^1 rotamer distribution. Deviations of the experimental $^3J(H^\alpha H^\beta)$ values of Tyr[4] and Trp[10] will be discussed in conjunction with the 3D structure of the molecule (see the Structure and Dynamics section). Temperature dependencies of backbone amide proton chemical shifts are in good agreement with the corresponding amide proton solvent accessibilities calculated from the rMD trajectory (Figure 5).

Solution Structure and Dynamics of *cyclo*[21,29]-[D-Cys[21]Cys[29]]-uPA$_{21-30}$. The 3D structure of peptide **4** is characterized by a hydrophobic cluster located on one side of the ring, involving amino acid residues Tyr[4], Phe[5], Ile[8], and Trp[10] and two type βI-turns centered at Lys[3], Tyr[4], Ser[6], and Asn[7], respectively (Figure 6). All of the hydrophobic residues (Tyr[4], Phe[5], Ile[8], and Trp[10]) participate in the formation of a hydrophobic cluster. Ile[8] is in the core of the cluster, with its side chain being shielded from the aqueous environment by the phenyl ring of Phe[5] and the indole moiety of Trp[10]. This finding is consistent with the distinct upfield shift observed for the chemical shifts of the methyl groups of the isoleucine side chain, suggesting these methyls to be located above the plane of aromatic ring systems (see section on NMR Assignment). However, the nature of the hydrophobic cluster is not as static as Figure 6 might suggest. As can be seen in the rMD simulations (Figure 4), Ile[8] displays remarkable flexibility around χ^1. According to one larger and one smaller $^3J(H^\alpha H^\beta)$ value (Table 3), Tyr[4] partially adopts the g^- and t rotamer, while in the rMD simulation only the g^+ rotamer is populated (Figure 4), allowing the formation of a hydrophobic cluster with Phe[5] (Figure 6). In contrast, the g^- rotamer enables a hydrophobic interaction with the methylenes of the lysine side chain, a feature also found in the corresponding ω-loop in the NMR solution structure of ATF.[14] The resulting spatial arrangement would still be consistent with the observed NOEs between the side chains of Lys[3] and Tyr[4] and could also account for the distinct upfield shift of the β, γ, and δ protons of the lysine side chain (see section on NMR Assignment). In the case of Trp[10], the experimental evidence (both $^3J(H^\alpha H^\beta)$ around 7.0 Hz, upper bound of $H^\alpha - H^\beta$ distance restraint violated) also indicated side chain rotation, albeit not reproduced in the rMD simulation (Figure 4). Rotation around χ^1 would bring the indole ring of Trp[10] into a position comparable to that observed for its counterpart in the solution structure of ATF. Obviously, the chosen time averaging regime for NOE-derived distance restraints using a memory decay time τ of 20 ps[21] does not allow for side chain rotational fluctuations large enough to correctly reproduce the experimental $^3J(H^\alpha H^\beta)$ values.

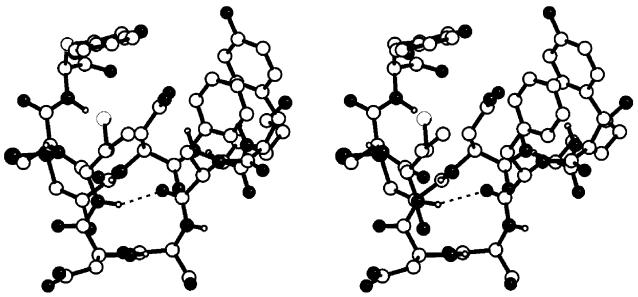

Figure 6. Stereoview of the NMR solution structure of *cyclo*[21,29][D-Cys[21]Cys[29]]-uPA$_{21-30}$ **4** in water.

In addition to the hydrophobic cluster, peptide **4** also displayed a regular secondary structure. A βI-turn (ideal ϕ,ψ dihedral values: $-60°$, $-30°$ ($i + 1$ position) and $-90°$, $0°$ ($i + 2$ position))[22,23] is centered at Lys[3] and Tyr[4] (Figures 6 and 7). The corresponding (i,$i + 3$) hydrogen bond is not populated to an appreciable extent, a phenomenon also encountered in 25% of the β-turns found in protein structures.[24] The turn is stabilized by a side chain−backbone hydrogen bond between Asn[2]O$^{\delta1}$ and the amide proton of Tyr[4], forming another turnlike structure known as "Asx turn".[25] In addition, the

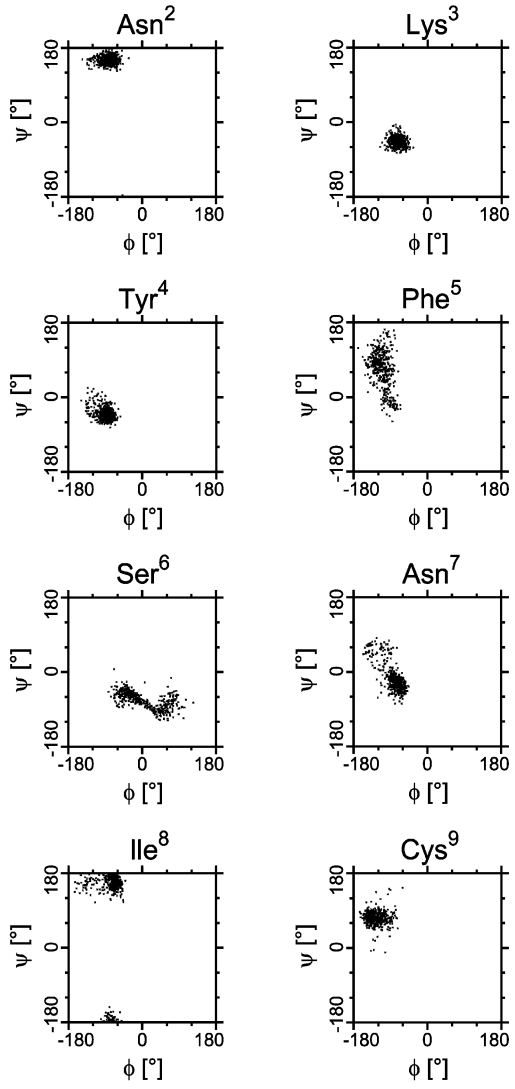

Figure 7. Ramachandran plots generated from the two 200 ps rMD simulations starting from different initial velocities.

Table 4. Populations of Hydrogen Bonds of *cyclo*[21,29][D-Cys^{21}Cys^{29}]-uPA$_{21-30}$ **4** in Water at 280 K Calculated from the RMD Trajectory

donor	acceptor	population[a,b]	donor	acceptor	population[a,b]
Asn^{2}H^N	Ile^{8}CO	76	Ser^{6}HO$^\gamma$	Phe^{5}CO	10
Asn^{2}H^N	Ser^{6}CO	23	Asn^{7}H^N	Ser^{6}O$^\gamma$	49
Lys^{3}H^N	Asn^{2}O$^{\delta1}$	42	Asn^{7}H^N	Phe^{5}CO	14
Tyr^{4}H^N	Asn^{2}O$^{\delta1}$	60	Ile^{8}H^N	Phe^{5}CO	59
Phe^{5}H^N	Asn^{2}O$^{\delta1}$	52			

[a] Hydrogen bonds are defined by a distance between donor and acceptor of $D_{A,D} \leq 2.8$ Å and an angle between the vectors NH and HO of $\delta = 180 \pm 60°$. [b] Existing hydrogen bond during simulation time (%).

Asn^{2}O$^{\delta1}$ hydrogen bond to Phe^{5}H^N provides a rational explanation for the weakly populated (i,$i+3$) hydrogen bond (52%) of this βI-turn (Table 4). Another type I β-turn is centered at Ser^6 and Asn^7, with the corresponding (i,$i+3$) hydrogen bond between Phe^{5}CO and Ile^{8}H^N populated in more than half of the rMD simulation time (Table 4). An equally populated hydrogen bond between Ser^{6}O$^\gamma$ and Asn^{7}H^N stabilizes the ψ_{i+1} angle of this turn. In the course of the rMD simulation, the Phe^5−Ser^6 amide bond rotates (Figure 7), giving rise to a weakly populated type γ-turn centered at Ser^6 with the ϕ_{i+1} angle stabilized by an additional side chain−backbone hydrogen bond between Phe^{5}CO and Ser^{6}H$^\gamma$ (Table 4). The ϕ,ψ pairs of this turn are close to their ideal values (70°,−70°). The observed arrangement of two consecutive type βI-turns is additionally stabilized by a strongly populated hydrogen bond between Asn^{2}H^N and Ile^{8}CO.

Agreement with Statistically Determined β-Turn Positional Preferences. The large body of experimental information on the 3D structure of proteins available in the Brookhaven Protein Data Bank[26] has enabled conformational and positional preferences of residues to be statistically determined.[27−31] Using a nonhomologous data set of 205 protein chains, Hutchinson and Thornton derived β-turn positional potentials for the 20 naturally occurring amino acids.[31] For position i of type βI-turns, they found a strong preference for side chains that can act as hydrogen bond acceptors (Asn, Asp, Cys, Ser, and His). These stabilize the turn by the formation of a hydrogen bond with the main chain nitrogen of the $i+2$ residue. Thereby, another turnlike structure known as Asx turn arises, made up by the side chain and main chain of residue i, together with the main chains of residues $i+1$ and $i+2$. For the remaining positions of type βI-turns, Hutchinson and Thornton found significant positional preferences for the following residues: $i+1$: Pro, Ser, Glu; $i+2$: Thr, Ser, Asn, Asp; $i+3$: Gly. Indeed, an Asx turn is observed for the βI-turn centered at Lys^3 and Tyr^4 of peptide **4**, bearing Asn^2 in position i. However, none of the other residues of this βI-turn (Lys^3 in $i+1$, Tyr^4 in $i+2$, and Phe^5 in $i+3$ position) displays significant propensity to appear in its respective position. In contrast, Ser^6 and Asn^7 in $i+1$ and $i+2$ positions, respectively, of the second βI-turn are in perfect agreement with the statistically derived preferences (see above). Ser^{6}O$^\gamma$ forms hydrogen bonds with Asn^{7}H^N and thereby stabilizes the ψ^{i+1} angle. As for position $i+2$, an analysis of high-resolution protein structures showed that Asn, along with Asp, Ser, and Thr, is more likely to adopt the backbone conformation required for this position ($\phi = -90°$, $\psi = 0°$).[32]

Comparison of *cyclo*[21,29][D-Cys^{21}Cys^{29}]-uPA$_{21-30}$ with the Solution Structure of ATF. *cyclo*[21,29][D-Cys^{21}Cys^{29}]-uPA$_{21-30}$ **4** and ATF of uPA display similar binding characteristics toward cellular uPAR. Thus, similar orientations of amino acids in ATF and in the synthetic uPA peptide, critical for receptor binding, can be expected. Amino acid residues mediating receptor binding encompass Tyr^{24}, Phe^{25}, Ile^{28}, and Trp^{30} within the ω-loop of ATF and the corresponding residues Tyr^4, Phe^5, Ile^8, and Trp^{10} in cyclic peptide **4**, as determined by alanine replacements. Superposition of peptide **4** with the solution structure of ATF[14] ($C^\alpha-C^\beta$ vectors of Phe, Tyr, and Ile were used) revealed that amino acid residues Tyr^{24} (Tyr^4 in the cyclic peptide), Phe^{25} (Phe^5), and Ile^{28} (Ile^8) adopt almost identical positions in space and orientations relative to each other (RMSD between $C^\alpha-C^\beta$ vectors of corresponding tyrosine, phenylalanine, and isoleucine residues is 0.6 Å; see also Figure 8). Trp^{30} (Trp^{10}), however, is found in different orientations in ATF and peptide **4**. In peptide **4**, Trp^{10} is located outside the cyclic backbone of the peptide, which confers considerable conformational flexibility to this C-terminal residue. Thus, Trp^{10} can participate in the formation of

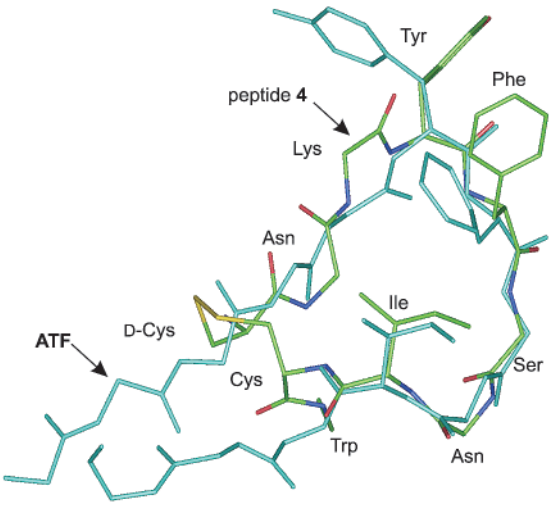

Figure 8. Superposition of the energy-minimized average structure of the receptor binding region of ATF with the NMR solution structure of *cyclo*[21,29][D-Cys^{21}Cys^{29}]-uPA$_{21-30}$ **4**.

the observed hydrophobic cluster, together with Tyr^4, Phe^5, and Ile^8.

Upon receptor binding, however, in peptide **4**, the conformational flexibility enables Trp^{10} to bring its indole in a position comparable to that found in ATF. Interestingly, the motif of Phe and Trp, separated by five amino acid residues in sequence, is among the essential features of uPAR binding peptide antagonists as identified by phage display technology; the consensus sequence derived from these linear peptides is XFXX-YLW.[11,15,18] The importance of proper spacing is further corroborated by the experimental finding that insertion of either Gly or β-Ala between Phe and Trp into the phage display peptides resulted in loss of its receptor binding function.[33] Furthermore, a manual alignment of peptide **4** and the above consensus sequence reveals the hydrophobic residues Ile^8 and the consensus Tyr to be located at equivalent positions. Thus, formation of a hydrophobic cluster between Phe and Ile (Tyr), as observed for peptide **4**, and appropriately spaced Trp, is essential to mediate high affinity binding of peptide **4** to cellular uPAR.

Further Modification of *cyclo*[21,29][D-Cys^{21}-Cys^{29}]-uPA$_{21-30}$ to Increase Stability toward Proteolytic Enzymes In Vivo. To explore whether *cyclo*[21,29][D-Cys^{21}Cys^{29}]-uPA$_{21-30}$ **4** is cytotoxic for cells, its effect on viability of various different human tumor cell lines was determined (Figure 9). uPAR expressing human fibrosarcoma, carcinoma, and promyelocytic cell lines was assessed. All of the cell lines tested survived when exposed up to 350 μM peptide **4** for 72 h. For HL-60 cells, a small decline in cell growth was observed with increasing amounts of peptide **4**. High-performance liquid chromatography (HPLC) analyses of peptide **4** from the cell culture supernatants demonstrated that the peptide remained stable during the incubation time. These results indicate the potential use of cyclic peptide **4** in cancer therapy to target uPAR-bearing cells, even in the high micromolar range.

Some positions in the peptide mimetics **3** and **4** are prone to tolerate substitutions of their side chains and/or stereochemical orientations, which opens up new vistas toward the design of highly active and stable uPA

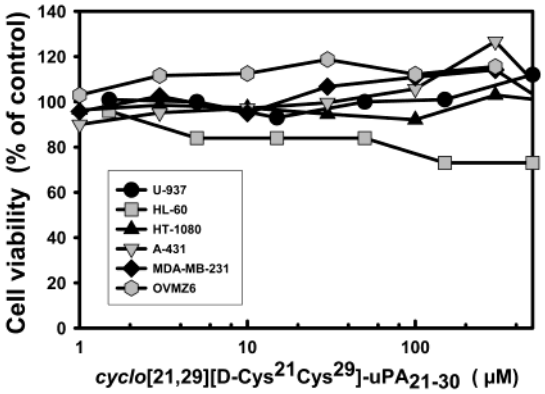

Figure 9. Effect of *cyclo*[21,29][D-Cys^{21}Cys^{29}]-uPA$_{21-30}$ on viability of different human tumor cells.

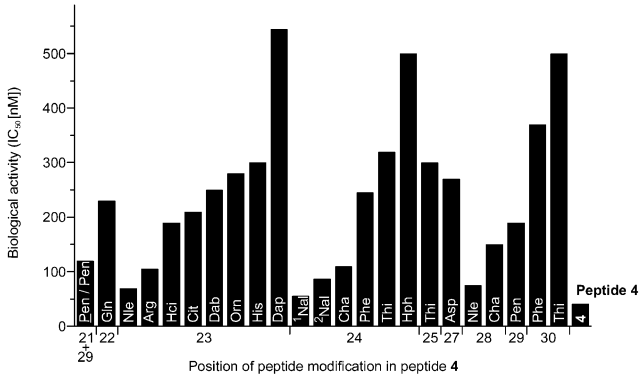

Figure 10. Biological activities of the most potent side chain modifications of *cyclo*[21,29][D-Cys^{21}Cys^{29}]-uPA$_{21-30}$. Influence of amino acid substitution in *cyclo*[21,29][D-Cys^{21}Cys^{29}]-uPA$_{21-30}$ **4** on the capacity to inhibit FITC-uPA/uPAR interaction as assessed by FACS and related toward the binding activity of peptide *cyclo*[21,29][D-Cys^{21}Cys^{29}]-uPA$_{21-30}$ **4**.

receptor antagonists. To obtain new peptidomimetics with prolonged biological action and high stability toward proteolytic attack in vivo, modifications of peptide **4** were undertaken by introducing nonnatural or isosteric amino acids to stabilize the molecule (Figure 10). For *cyclo*[21,29][D-Cys^{21}Cys^{29}]-uPA$_{21-30}$ **4**, the effect of introducing unnatural or natural amino acids with an isofunctional, isosteric molecular frame or comparable space requirement on the inhibitoric capacity was determined. To draw conclusions how the length of the amino acid side chain affects the biological activity, a systematic replacement of amino acids was used, such as replacing lysine in position 23 by ornithine, diaminobutyric acid, or diaminopropionic acid. The aromatic amino acids Phe and Tyr were replaced by a series of unnatural aromatic or hydrophobic amino acids, such as naphthylalanine Nal, thienylalanine Thi, and cyclohexylalanine Cha. The inhibitory potencies toward the uPA receptor of these unnatural amino acid-containing uPA analogues varied between weak and potent. The IC$_{50}$ values of the most potent receptor binding peptides ranging from 0.04 μM to over 1 μM are depicted in Figure 10.

A high degree of inhibition was obtained with the hydrophobic amino acid Nle-containing analogue in position 23 with an IC$_{50}$ value of 0.06 μM, and the 1- and 2-naphthylalanine-containing analogues in position 24, with IC$_{50}$ values of 0.05 and 0.08 μM, respectively. It is interesting to note that removal of the positive

charge at residue 23 by incorporation of Nle yielded the potent inhibitor *cyclo*[21,29][D-Cys^{21}Nle^{23}Cys^{29}]-uPA$_{21-30}$. This suggests that hydrophobic interaction at amino acid position 23 of the uPA peptide with the uPA receptor is important for efficient binding. Shortening of the side chain in position 23 and retaining a positive charge lead to ligands with decreased binding affinity.

The replacement of Lys by certain unnatural amino acids such as Nle, Dab, Orn, and Dap yielded potent uPAR antagonists (with the Nle derivative being the most potent; Figure 10), which are highly resistant to proteolytic confrontation with plasmin (which is present in plasma and tumor tissue). Whereas *cyclo*[21,29][D-Cys^{21}Cys^{29}]-uPA$_{21-30}$ **4** displayed resistance to plasmin only up to 1 h of incubation, peptide **4** modified at position 23 by Nle, Orn, Dab, or Dap was completely resistant to proteolysis. No detectable degradation of the peptide *cyclo*[21,29][D-Cys^{21}Cys^{29}]-uPA$_{21-30}$ **4** and its lysine modifications was seen in the presence of uPA. Stability testing showed that *cyclo*[21,29][D-Cys^{21}Cys^{29}]-uPA$_{21-30}$ **4** and its lysine modifications at position 23 (Nle, Orn; Dab, Dap) were highly resistant to proteolytic degradation in plasma or serum while *cyclo*[19,31]-uPA$_{16-32}$ was less stable. Incubation of *cyclo*[19,31]-uPA$_{16-32}$ with serum or plasma over a period of 10−15 min, necessary for addition of the peptide to serum/plasma and immediate separation by HPLC, was sufficient for degrading roughly 80% of the peptide. After 1 h (37 °C) of incubation in serum/plasma, peptide *cyclo*[19,31]-uPA$_{16-32}$ was completely degraded. In contrast, in serum/plasma *cyclo*[21,29][D-Cys^{21}Cys^{29}]-uPA$_{21-30}$ **4** and its lysine modifications at position 23 were stable over a period of 24 h (37 °C).

In a recent study, *cyclo*[21,29][D-Cys^{21}Cys^{29}]-uPA$_{21-30}$ **4** and its Nle derivative were tested in nude mice for their potency to inhibit tumor growth and intraperitoneal spread of human ovarian cancer cells (Sato, S.; et al. Manuscript submitted for publication). Intraperitoneal administration of either cyclic peptide (20 mg peptide/kg; 1× daily for 37 days) into the tumor-bearing nude mice resulted in a significant reduction of tumor weight and spread within the peritoneum as compared to the untreated control group. Thus, both peptides are promising novel compounds to interfere with dissemination of human carcinoma cells in vivo.

Conclusions

Optimization of the sequence and composition of uPA-derived lead peptide *cyclo*[19,31][D-Cys^{19}]-uPA$_{19-31}$ and stepwise reduction of its size, starting from the receptor binding site of uPA, generated uPA analogue peptide *cyclo*[21,29][D-Cys^{21}Cys^{29}]-uPA$_{21-30,}$ displaying a urokinase receptor binding capacity close in order to that of parent uPA. This uPA peptide structure, resolved by NMR, exhibited features allowing further uPA receptor binding optimization and stability. Stability against proteolytic cleavage in vivo was achieved by substitution of lysine 23 by the nonnatural amino acid norleucine leading to peptide *cyclo*[21,29][D-Cys^{21}Nle^{23}-Cys^{29}]-uPA$_{21-30}$. Such small cyclic peptides, which mimic the structure and activity of the binding site of naturally occurring tumor-associated uPA for uPAR, may serve as novel therapeutic agents to block cancer metastasis.

Experimental Section

Starting Materials for Solid Phase Syntheses. Trityl chloride polystyrene resin (PepChem, Tübingen, Germany) and Rink Amide MBHA resin (NovaBiochem, Schwalbach, Germany) were used for peptide syntheses. *S*-Trityl-2-mercaptoacetic-, *S*-trityl-3-mercaptopropionic, and *S*-trityl-*rac*-2-mercaptolactic acid were prepared from the free thiol compounds (Merck, Darmstadt, and Fluka, Deisenhofen, Germany) and trityl alcohol (Sigma-Aldrich, Deisenhofen, Germany) applying methods described earlier.[34] Fluorenylmethoxycarbonyl-(Fmoc) amino acids were purchased from Alexis (Grünberg, Germany), NovaBiochem (Schwalbach, Germany), Bachem (Heidelberg, Germany), or MultSynTech (Witten, Germany). All reagents and solvents were reagent grade or better and used without further purification.

Peptide Synthesis and Purification. Linear peptides were synthesized using a MultiSynTech multiple peptide synthesizer, model SyRo II. Applying an orthogonal Fmoc strategy,[35,36] the amino acid side chains were protected with trityl-(for Asn, Cys, Gln, and His), *tert*-butyloxycarbonyl-(Boc, for Lys and Trp), *tert*-butyl-(for Asp, Glu, Ser, Thr, and Tyr), and 2,2,5,5,7,8-pentamethylchroman-6-sulfonyl-(Pmc) or 2,2,4,6,7-pentamethyl-dihydrobenzofuran-5-sulfonyl-(Pbf, for Arg) groups. Couplings were performed twice for 1 h at room temperature in *N*-methyl-pyrrolidone (NMP) using a 3-fold excess of *O*-(benzotriazol-1-yl)-*N*,*N*,*N*′,*N*′-tetramethyluronium tetrafluoroborate (TBTU)/*N*-hydroxybenzotriazole (HOBt)/Fmoc-amino acid with 2.8 equiv of DIEA in NMP. The Fmoc group was removed by sequential treatment of the resins with an excess of 20% piperidine in dimethylformamide (DMF), for 5 and 15 min, respectively. Acetate capping was achieved by treatment with 5% acetic anhydride/DIEA in NMP for 30 min. Cleavage of the peptides, removal of the side chain protecting groups, and workup were performed as follows: (i) Treatment with 82.5% trifluoroacetic acid (TFA)/5% phenol/2.5% ethanedithiol/5% thioanisole/5% water (0 °C for 1 h; room temperature for 1 h). In the case of Pmc-protected Arg, peptides were treated for an additional 12 h (room temperature). The crude peptides were precipitated in diethyl ether at −30 °C, dissolved in methanol, precipitated as before, redissolved in *t*BuOH, and lyophilized. (ii) Treatment with 90% TFA/7% triisopropylsilane (TIPS)/3% water (room temperature, 3 × 15 min) and subsequent evaporation. The resulting crude peptides were suspended in water (0.1−0.3 mg/mL) and cooled with ice, and 20% dimethyl sulfoxide (DMSO) (v/v) was added. After the oxidation reaction was completed, according to the HPLC control (12 h for Cys/Cys derivatives, up to 3 days in the case of Pen/Pen bridging), the solvent was removed under reduced pressure, and the resulting white solid was dissolved in DMSO, diluted with an equal volume of water, filtered, and purified by HPLC using a Beckman Instruments System Gold or a Pharmacia Biotech Series 900 with a reverse phase C-18 column (YMC-Pack ODS/A column) employing water and ACN with 0.1% TFA as eluents.

MS and Quantification of Target Peptides. Electrospary ionization (ESI)-MS and RP-HPLC-ESI-MS analyses were performed using a Finnigan LCQ-ESI Spectrometer coupled to a Hewlett-Packard HP1100 HPLC-System. Amino acid analysis was performed by the ninhydrin method using a Beckman Instruments analyzer system 6300 after having hydrolyzed the peptides by the TFA−HCl vapor phase method as described earlier.[11]

NMR Spectroscopy. All NMR spectra were acquired on a Bruker DMX600 spectrometer and processed and analyzed using the X-WINNMR software. A set of 1D spectra were acquired at the following temperatures: 275, 276, 278, 280, 282, 284, and 285 K. COSY and NOESY spectra were acquired in water with 1024 and 512 complex points in *t*2 and *t*1, respectively, performing 64 scans per increment. A mixing time of 80 ms was chosen for the NOESY. Water suppression was accomplished using WATERGATE. The E.COSY spectrum was recorded in D_2O at a resolution of 4096 (*t*2) × 256 (*t*1) complex points, with 48 scans per increment. All 2D spectra were recorded at 280 K with a 12.2 mM peptide sample.

NOE-Derived Distance Restraints. NOE cross-peaks were converted into distance restraints d_{NOE} according to their integrated volumes using the two spin approximation. The lower and upper bound of each distance restraint was set to 0.9 d_{NOE} and 1.1 d_{NOE}, respectively. The average intensity of NOEs between geminal methylene protons (corresponding to a distance of 1.8 Å) was used for calibration. Standard corrections for center averaging were applied.[37]

Coupling Constants. $^3J(H^NH^\alpha)$ was obtained from the COSY spectrum using the methodology pioneered by Kim and Prestegard.[38] $^3J(H^\alpha H^\beta)$ was extracted from the E.COSY recorded in D_2O.

Amide Proton Temperature Coefficients. Temperature dependencies of the backbone amide proton chemical shifts were calculated from the above temperature series of ^1H 1D experiments.

Structure Calculations. Structure calculations consisted of a two step procedure involving conformational space sampling followed by refinement of the obtained 3D structure. In vacuo conformational space sampling was performed with the X-PLOR 3.5 program employing a standard simulated annealing (SA) protocol.[21] A random conformation with optimized covalent bond geometries was used as the initial structure for all calculations. NOE-derived distances as well as $^3J(H^NH^\alpha)$ coupling constants were employed as restraints. Ten low-energy conformations out of a total of 20 generated structures were selected for analysis of the agreement with the NMR-derived restraints. A structural representative of the ensemble of low-energy structures was then chosen and refined in extensive MD simulations. To this end, the representative was placed in a 35 Å cubic simulation cell soaked with 1345 water molecules. The simulation cell was then energy-minimized and slowly heated to the target temperature of 280 K. After equilibration, 200 ps rMD was performed. Solely NOE-derived distances were employed, acting as time-averaged distance restraints[39−42] with a memory decay time of $\tau = 20$ ps.[42] To obtain average properties, the above simulation protocol was carried out twice, starting from different initial velocities. Finally, one MD simulation in water was resumed in absence of restraints to probe the stability of the structure (fMD). All MD simulations were performed with the DISCOVER 98 program (Molecular Simulations Inc.) using an in-house C extension handling the time averaging of distance restraints.

Flow Cytofluorometry (FACS). The capacity of synthetic peptides to inhibit uPA/uPAR interaction was assessed by FACS analysis with the Becton Dickinson FACS calibur flow cytofluorometer (low power argon laser excitation at 488 nm).[10−12,43] Briefly, human U937 cells—stimulated with phorbol-12-myristate-13-acetate (PMA, 1 mM) for 48 h to induce overexpression of uPAR—were treated with 50 mM glycine−HCl, 0.1 M NaCl, pH 3.0, to dissociate endogenous receptor-bound uPA (1 min, room temperature). Subsequently, the acidic buffer was neutralized by an appropriate volume of 0.5 M HEPES−100 mM NaCl, pH 7.5. The cells were washed, centrifuged, and resuspended in phosphate-buffered saline (PBS)/0.1% bovine serum albumin (BSA) and then adjusted to 10^6 cells/mL. Different from previous reports in which FITC-uPA and competitive agents were incubated simultaneously with the uPAR-bearing U937 cells,[12,44] the still living cells were preincubated with synthetic peptides (45 min, room temperature) prior to addition of 25 ng of FITC-conjugated HMW-uPA and allowed to incubate for another 30 min at room temperature. Without any further wash, cell-associated fluorescence was determined by FACS and expressed as fluorescence mean channel. Reduction in cell-associated fluorescence indicated receptor binding activity of the peptide in question.

Cell Viability Assays. The A-431 (epidermoid carcinoma) cell line was obtained from American Type Culture Collection. The MDA-MB-231 BAG cell line (human breast cancer adenocarcinoma cell transfected with BAG vector and X-Gal) was a gift from Nils Brünner, Finsen Laboratory, Copenhagen, Denmark.[45] The OV-MZ-6 (human ovarian cancer cell) cells were established from a patient with advanced serous cystadenocarcinoma of the ovary.[46] Cell lines HT-1080 (fibrosarcoma), A-431, MDA-MB-231 BAG, and OV-MZ-6 were grown as adherent cells in Dulbecco's modified Eagle's medium (DMEM). Promyelocytic cell lines HL-60 and U-937 were grown as suspension cells in RPMI-1640. Media were supplemented with 10% fetal calf serum (FCS) and 2 mM Glutamax and cells grown at 37 °C in a humidified atmosphere containing 5% CO_2. Viability studies on adherent cells were performed in 96 well plates in the presence of increasing concentrations of *cyclo*[21,29][D-Cys^{21}Cys^{29}]-uPA$_{21-30}$ **4** in DMEM/FCS. After 3 days in culture, the cells were inactivated in 10% trichloroacetic acid and stained with 0.4% sulforhodamine B in 1% acetic acid. The bound dye was dissolved in 200 μL of 10 mM unbuffered TRIS, and the optical density was measured at 515 nm using an enzyme-linked immunosorbent assay microplate reader (Mediators PhL). Untreated control wells were assigned a value of 100%, and the IC_{50} was defined as this dose of peptide required to inhibit color development by 50% of the control value. Viability of suspension cells HL-60 and U-937 was measured using the Alamar Blue Assay, which also assesses the metabolic activity of the cells, conforming with the manufacturer's (Biosource International, CA) recommendation.

Peptide Stability in Human Serum and Plasma. To prepare human serum, venous blood from healthy donors was coagulated in a polypropylene tube (45 min, 37 °C) and centrifuged (1200*g*, 12 min, room temperature). Plasma from healthy donors was prepared by addition of 1000 I. E. heparin to 10 mL of venous blood followed by low speed centrifugation to separate blood cells from plasma. Both serum and plasma were stored at −20 °C until use. Peptides were dissolved in water (1 mg/mL; with exception of the Nle-containing analogue of peptide **4** in position 23: 0.3 mg/mL) and stored at −20 °C until use. For stability tests, 5 μg of the peptides was added to 100 μL of serum or plasma and incubated for different periods of time at 37 °C. Before further processing by HPLC, serum and plasma were centrifuged at 16 000*g* (5 min, 4 °C) and the supernatants were subjected to Oasis HLB solid phase extraction cartridges (Waters, Eschborn, Germany; 1 cm^3/10 mg). For this purpose, HLB cartridges were washed with 1 mL of methanol, each, followed by 1 mL of water and then loaded with 100 μL of test solution diluted with 900 μL of PBS. The extraction cartridge was then washed with 5% methanol in water followed by 1 mL of methanol. The first eluting 200 μL of fluid was disposed, and the following 500 μL was collected, 500 μL of PBS was added and analyzed by HPLC using a reversed phase C-18 column (YMC-5 C_{18}). Peptides were eluted within 30 min by applying a 20−60% gradient composed of H_2O/0.1% TFA and acetonitrile/0.1% TFA.

Exposure of Cyclic Peptides to Plasmin and uPA. To test for degradation of cyclic peptides by plasmin, 5 μg of peptide was incubated with 0.01 U (≈4 μg) of plasmin (Sigma, Deisenhofen, Germany) in 100 mM sodium phosphate, pH 7.5 (end-volume: 100 μL; 1 h; 37 °C). In the case of uPA, 5 μg of peptide was incubated with 100 U (≈1 μg) of uPA (Rheotromb 500 000, Curasan Pharma GmbH, Kleinostheim, Germany) in PBS (end-volume: 100 μL; 1 h; 37 °C). The peptides were further processed by HPLC as described above.

Acknowledgment. The excellent technical assistance of N. Potthoff and C. Schnelldorfer is gratefully acknowledged. Part of this work was supported by grants of the Sonderforschungsbereich 469 and the Sonderforschungsbereich 456 of the Deutsche Forschungsgemeinschaft (DFG). H.K. thanks also the Fonds der Chemischen Industrie for financial support.

References

(1) Edwards, D. R.; Murphy, G. Proteases—invasion and more. *Nature* **1998**, *394*, 527−528.
(2) Johnsen, M.; Lund, L. R.; Rømer, J.; Almholt, K.; Danø, K. Cancer invasion and tissue remodeling: common themes in proteolytic matrix degradation. *Curr. Opin. Cell Biol.* **1998**, *10*, 667−671.
(3) Koblinski, J. E.; Ahram, M.; Sloane, B. F. Unraveling the role of proteases in cancer. *Clin. Chim. Acta* **2000**, *291*, 113−135.

(4) Andreasen, P. A.; Egelund, R.; Petersen, H. H. The plasminogen activation system in tumor growth, invasion, and metastasis. *Cell. Mol. Life Sci.* **2000**, *57*, 25−40.
(5) Foekens, J. A.; Peters, H. A.; Look, M. P.; Portengen, H.; Schmitt, M.; Kramer, M. D.; Brünner, N.; Jänicke, F.; Gelder, M. E. M.-v.; Henzen-Logmans, S. C.; Putten, W. L. J. V.; Klijn, J. G. M. The urokinase system of plasminogen activation and prognosis in 2780 breast cancer patients. *Cancer Res.* **2000**, *60*, 636−643 and references therein.
(6) Schmitt, M.; Wilhelm, O. G.; Reuning, U.; Krüger, A.; Harbeck, N.; Lengyel, E.; Graeff, H.; Gänsbacher, B.; Kessler, H.; Bürgle, M.; Stürzebecher, J.; Sperl, S.; Magdolen, V. The urokinase plasminogen activator system as a novel target for tumour therapy. *Fibrinolysis Proteolysis* **2000**, *14*, 114−132.
(7) Mazar, A. P. The urokinase plasminogen activator receptor (uPAR) as a target for the diagnosis and therapy of cancer. *Anti-Cancer Drugs* **2001**, *12*, 387−400.
(8) Muehlenweg, B.; Sperl, S.; Magdolen, V.; Schmitt, M.; Harbeck, N. Interference with the urokinase plasminogen activator (uPA) system: A promising therapy concept for solid tumors. *Exp. Opin. Biol. Ther.* **2001**, *1*, 683−691.
(9) Appella, E.; Robinson, E. A.; Ullrich, S. J.; Stoppelli, M. P.; Corti, A.; Cassani, G.; Blasi, F. The receptor-binding sequence of urokinase. A biological function for the growth-factor module of proteases. *J. Biol. Chem.* **1987**, *262*, 4437−4440.
(10) Magdolen, V.; Rettenberger, P.; Koppitz, M.; Goretzki, L.; Kessler, H.; Weidle, U. H.; König, B.; Graeff, H.; Schmitt, M.; Wilhelm, O. Systematic mutational analysis of the receptor-binding region of the human urokinase-type plasminogen activator. *Eur. J. Biochem.* **1996**, *237*, 743−751.
(11) Bürgle, M.; Koppitz, M.; Riemer, C.; Kessler, H.; König, B.; Weidle, U. H.; Kellermann, J.; Lottspeich, F.; Graeff, H.; Schmitt, M.; Goretzki, L.; Reuning, U.; Wilhelm, O. G.; Magdolen, V. Inhibition of the interaction of urokinase-type plasminogen activator (uPA) with its receptor (uPAR) by synthetic peptides. *Biol. Chem.* **1997**, *378*, 231−237.
(12) Magdolen, V.; Bürgle, M.; Prada, N. A.; Schmiedeberg, N.; Riemer, C.; Schroeck, F.; Kellermann, J.; Degitz, K.; Wilhelm, O. G.; Schmitt, M.; Kessler, H. Cyclo^{19,31}[D-Cys^{19}]-uPA$_{19-31}$ is a potent competitive antagonist of the interaction of urokinase-type plasminogen activator with its receptor (CD87). *Biol. Chem.* **2001**, *382*, 1197−1205.
(13) Kessler, H. Conformation and biological activity of cyclic peptides. *Angew. Chem., Int. Ed.* **1982**, *21*, 512−523.
(14) Hansen, A. P.; Petros, A. M.; Meadows, R. P.; Nettesheim, D. G.; Mazar, A. P.; Olejniczak, E. T.; Xu, R. X.; Pederson, T. M.; Henkin, J.; Fesik, S. W. Solution structure of the amino-terminal fragment of urokinase-type plasminogen activator. *Biochemistry* **1994**, *33*, 4847−4864.
(15) Goodson, R. J.; Doyle, M. V.; Kaufman, S. E.; Rosenberg, S. High-affinity urokinase receptor antagonists identified with bacteriophage peptide display. *Proc. Natl. Acad. Sci. U.S.A.* **1994**, *91*, 7129−7133.
(16) Guo, Y.; Higazi, A. A.; Arakelian, A.; Sachais, B. S.; Cines, D.; Goldfarb, R. H.; Jones, T. R.; Kwaan, H.; Mazar, A. P.; Rabbani, S. A. A peptide derived from the nonreceptor binding region of urokinase plasminogen activator (uPA) inhibits tumor progression and angiogenesis and induces tumor cell death in vivo. *FASEB J.* **2000**, *14*, 1400−1410.
(17) Ploug, M.; Østergaard, S.; Gårdsvoll, H.; Kovalski, K.; Holst-Hansen, C.; Holm, A.; Ossowski, L.; Danø, K. Peptide-derived antagonists of the urokinase receptor. Affinity maturation by combinatorial chemistry, identification of functional epitopes, and inhibitory effect on cancer cell intravasation. *Biochemistry* **2001**, *40*, 12157−12168.
(18) Fong, S.; Doyle, M. V.; Goodson, R. J.; Drummond, R. J.; Stratton, J. R.; McGuire, L.; Doyle, L. V.; Chapman, H. A.; Rosenberg, S. Random peptide bacteriophage display as a probe for urokinase receptor ligands. *Biol. Chem.* **2002**, *383*, 149−158.
(19) Braun, D.; Wider, G.; Wüthrich, K. Sequence-corrected ^{15}N "random coil" chemical shifts. *J. Am. Chem. Soc.* **1994**, *116*, 8466−8469.
(20) Merutka, G.; Dyson, H. J.; Wright, P. E. "Random coil" ^{1}H chemical shifts obtained as a function of temperature and trifluoroethanol concentration for the peptide series GGXGG. *J. Biomol. NMR* **1995**, *5*, 14−24.
(21) Nilges, M.; Clore, G. M.; Gronenborn, A. M. Determination of three-dimensional structures of proteins from interproton distance data by dynamical simulated annealing from a random array of atoms. Circumventing problems associated with folding. *FEBS Lett.* **1988**, *239*, 129−136.
(22) Mueller, G.; Gurrath, M.; Kurz, M.; Kessler, H. βVI turns in peptides and proteins: A model peptide mimicry. *Proteins*: *Struct., Funct., Genet.* **1993**, *15*, 235−251.
(23) Richardson, J. S. The anatomy and taxonomy of protein structure. *Adv. Protein Chem.* **1981**, *34*, 167−339.
(24) Lewis, P. N.; Momany, F. A.; Scheraga, H. A. Chain reversals in proteins. *Biochim. Biophys. Acta* **1973**, *303*, 211−229.
(25) Rees, D. C.; Lewis, M.; Lipscomb, W. N. Refined crystal structure of carboxypeptidase A at 1.54 Å resolution. *J. Mol. Biol.* **1983**, *168*, 367−387.
(26) Bernstein, F. C.; Koetzle, T. F.; Williams, G. J. B.; Meyer, E. F., Jr.; Brice, M. D.; Rodgers, R. D.; Kennard, O.; Shimanouchi, T.; Tasumi, M. The Protein Data Bank: a computer-based archival file for macromolecular structures. *J. Mol. Biol.* **1977**, *112*, 535−542.
(27) Levitt, M. Conformational preferences of amino acids in globular proteins. *Biochemistry* **1978**, *17*, 4277−4285.
(28) Gray, T. M.; Matthews, B. W. Intrahelical hydrogen bonding of serine, threonine and cysteine residues within α-helixes and its relevance to membrane-bound proteins. *J. Mol. Biol.* **1984**, *175*, 75−81.
(29) Thornton, J. M.; Sibanda, B. L.; Edwards, M. S.; Barlow, D. J. Analysis, design and modification of loop regions in proteins. *BioEssays* **1988**, *8*, 63−69.
(30) Wilmot, C. M.; Thornton, J. M. Analysis and prediction of the different types of β-turn in proteins. *J. Mol. Biol.* **1988**, *203*, 221−232.
(31) Hutchinson, E. G.; Thornton, J. M. A revised set of potentials for β-turn formation in proteins. *Protein Sci.* **1994**, *3*, 2207−2216.
(32) Laskowski, R. A.; MacArthur, M. W.; Moss, D. S.; Thornton, J. M. PROCHECK: a program to check the stereochemical quality of protein structures. *J. Appl. Crystallogr.* **1993**, *26*, 283−291.
(33) Ploug, M.; Østergaard, S.; Hansen, L. B. L.; Holm, A.; Danø, K. Photoaffinity labeling of the human receptor for urokinase-type plasminogen activator using a decapeptide antagonist. Evidence for a composite ligand-binding site and a short interdomain separation. *Biochemistry* **1998**, *37*, 3612−3622.
(34) Zee-Cheng, K.-Y.; Cheng, C.-C. Experimental antileukemic agents. Preparation and structure−activity study of S-tritylcysteine and related compounds. *J. Med. Chem.* **1970**, *13*, 414−418.
(35) Carpino, L. A.; Han, G. Y. 9-Fluorenylmethoxycarbonyl amino-protecting group. *J. Org. Chem.* **1972**, *37*, 3404−3409.
(36) Fields, G. B.; Noble, R. L. Solid-phase peptide synthesis utilizing 9-fluorenylmethoxycarbonyl amino acids. *Int. J. Pept. Protein Res.* **1990**, *35*, 161−214.
(37) Wüthrich, K.; Billeter, M.; Braun, W. Pseudostructures for the 20 common amino acids for use in studies of protein conformations by measurements of intramolecular proton−proton distance constraints with nuclear magnetic resonance. *J. Mol. Biol.* **1983**, *169*, 949−961.
(38) Kim, Y.; Prestegard, J. H. Measurement of vicinal couplings from cross-peaks in COSY spectra. *J. Magn. Reson.* **1989**, *84*, 9−13.
(39) Torda, A. E.; Scheek, R. M.; van Gunsteren, W. F. Time-dependent distance restraints in molecular dynamics simulations. *Chem. Phys. Lett.* **1989**, *157*, 289−294.
(40) Torda, A. E.; Scheek, R. M.; van Gunsteren, W. F. Time Averaged NOE Distance Restraints Applied to Tendamista. *J. Mol. Biol.* **1990**, *214*, 223−230.
(41) Pearlman, D. A.; Kollman, P. A. Are time-averaged restraints necessary for nuclear magnetic resonance refinement? A model study for DNA. *J. Mol. Biol.* **1991**, *220*, 457−479.
(42) Nanzer, A. P.; van Gunsteren, W. F.; Torda, A. E. Parametrisation of time-averaged distance restraints in MD simulations. *J. Biomol. NMR* **1995**, *6*, 313−320.
(43) Guthaus, E.; Bürgle, M.; Schmiedeberg, N.; Hocke, S.; Eickler, A.; Kramer, M. D.; Sweep, C. G. J.; Magdolen, V.; Kessler, H.; Schmitt, M. uPA-Silica-Particles (SP-uPA): A novel analytical system to investigate uPA-uPAR-interaction and to test synthetic uPAR-antagonists as potential cancer therapeutics. *Biol. Chem.* **2002**, *383*, 207−216.
(44) Kobayashi, H.; Schmitt, M.; Goretzki, L.; Chucholowski, N.; Calvete, J.; Kramer, M.; Günzler, W. A.; Jänicke, F.; Graeff, H. Cathepsin B efficiently activates the soluble and the tumor cell receptor-bound form of the proenzyme urokinase-type plasminogen activator (pro-uPA). *J. Biol. Chem.* **1991**, *266*, *5147−5152*.
(45) Brünner, N.; Thompson, E. W.; Spang-Thomsen, M.; Rygaard, J.; Danø, K.; Zwiebel, J. A. lacZ transduced human breast cancer xenografts as an in vivo model for the study of invasion and metastasis. *Eur. J. Cancer* **1992**, *28A*, 1989−1995.
(46) Fischer, K.; Lutz, V.; Wilhelm, O.; Schmitt, M.; Graeff, H.; Heiss, P.; Nishiguchi, T.; Harbeck, N.; Kessler, H.; Luther, T.; Magdolen, V.; Reuning, U. Urokinase induces proliferation of human ovarian carcinoma cells: Characterization of structural elements required for growth factor function. *FEBS Lett.* **1998**, *438*, 101−105.

JM020254Q